Indian J Phys (January 2021) 95(1):89–97
https://doi.org/10.1007/s12648-019-01678-2

ORIGINAL PAPER

Importance of heat generation in chemically reactive flow subjected to convectively heated surface

W A Khan[1,2]*, H Sun[1], M Shahzad[2,3], M Ali[2,3], F Sultan[2,3] and M Irfan[4]

[1]School of Mathematics and Statistics, Beijing Institute of Technology, Beijing 100081, China

[2]Department of Mathematics, Mohi-ud-Din Islamic University, Nerian Sharif 12010, Azad Kashmir, Pakistan

[3]Department of Mathematics and Statistics, Hazara University, Mansehra 21300, Pakistan

[4]Department of Mathematics, Quaid-I-Azam University, Islamabad 44000, Pakistan

Received: 25 April 2019 / Accepted: 30 September 2019 / Published online: 13 January 2020

Abstract: Our main emphasis here is to scrutinize the Lorentz's force aspects on the flow of cross-fluid in cylindrical surface. More specifically, heat transfer features are examined subject to heat sink–source and radiative flux. Furthermore, aspects of quartic autocatalysis analysis are considered. Non-dimensional variables are introducing to develop the physical model. The physical problem by employing Bvp4c scheme. Influences of rheological parameters for concentration, temperature and velocity are discussed. Additionally, computational analysis for Nusselt number and skin friction coefficient is presented through tables.

Keywords: Time-dependent cross-fluid flow; Thermal radiation; Heat generation/absorption parameter; Heterogeneous–homogeneous reactions

PACS Nos.: 47.10.A−; 44.05.+e; 44.10.+i; 44.05; 44.40.+a

List of symbols

u, v	Velocity components
x	Distance along the axial direction
r	Distance along the radial direction
η	Local similarity variable
$b(t)$	Radial of cylinder
$B(t)$	Strength of magnetic field
c, b_0	Positive constants
v	Kinematics viscosity
T_∞	Ambient fluid temperature
Γ	Time material constant
T_w	Surface temperature
ρ_f	Fluid density
$\lambda_1 > 0$	Stretching cylinder
$\lambda_1 < 0$	Shrinking cylinder
n	Power law index
T	Fluid temperature
t	Time
σ^*	Stefan–Boltzmann
α_m	Thermal diffusivity
D_A, D_B	Diffusion coefficient
$(\rho c)_f$	Heat capacity of fluid
ρ_f	Fluid density
Q_0	Heat generation/absorption parameter
$U_w(x,t)$	Stretching velocity
$U_e(x,t)$	Free stream velocity
B_0	Magnetic field strength
S	Velocity ratio parameter
λ_1	Velocity ratio parameter
We	Local Weissenberg number
A	Unsteadiness parameter
Λ	Heat source–sink parameter
θ_w	Temperature ratio parameter
N_R	Radiation parameter
Pr	Prandtl number
S	Dimensionless suction parameter
K_s	Heterogeneous strength of reaction parameter
K	Strength coefficient of homogenous reaction
γ	Thermal Biot number
M	Magnetic parameter
Sc	Schmidt number
f	Dimensionless velocities

*Corresponding author, E-mail: waqar_qau@yahoo.com; waqarazeem@bit.edu.cn

© 2020 IACS

θ	Dimensionless temperature
ϕ	Dimensionless concentration
Re	Local Reynolds number
C_f	Skin friction
Nu_x	Local Nusselt number

1. Introduction

Non-Newtonian materials as compared to viscous liquids are more efficient in various physiological, engineering and industrial processes. Asphalts, biological solutions, paints and glues are some examples of nonlinear materials. More specifically, most of the liquids used in food and chemical industries are non-Newtonian liquids [1, 2]. Consequently, numerous relations were introduced in the literature to analyze the rheological properties of nonlinear materials. Cross-fluid model is one of these relations, which describes the shear-thinning features of liquids. Hayat et al. [3] considered properties of cross-material flow for stretched surface. Khan et al. [4] numerically analyzed heat transfer characteristics for cross-fluid. Khan et al. [5] securitized properties of static–moving wedge for cross-material. Manzur et al. [6] studied aspects of opposing and assisting flow for radiative cross-fluid. Sultan et al. [7] reported rheological analysis for 3D flow cross-fluid in the presence of nanomaterials.

A chemical reaction takes place, when the evident number of molecules of countable chemical species assumes a new form by changing the configuration of these atoms. Several reaction systems [8–28] comprise homogeneous/heterogeneous reactions, for example, in combustion, biochemical frameworks and catalysis. Heterogeneous reactions take place in different phase space (e.g., solid–gas space), while the homogeneous reactions have the same phase space. Furthermore, chemical reactions are applied as the part of applications such as food processing, rusting of iron, fog formation and several others. The aspects of nanoparticles and chemical mechanisms on generalized Burgers fluid flow over stretched surface have been inspected by Khan et al. [29]. Khan et al. [30] performed homogeneous–heterogeneous reactions and nonlinear thermal radiation solved numerically by a variable thicked surface. Sadiq et al. [31] observed chemically radiating flow toward heated surface of Maxwell liquid. Mahanthesh et al. [32] detected the properties of radiative flow by utilizing nanoparticles across permeable vertical plate. Hayat et al. [33] studied about reaction and convective flow between two rotating disks. Kumar et al. [34] analyzed the heat–mass transport behavior of chemically reacting of two different Casson and Maxwell fluids. Ramesh et al. [35] deliberated features of revised no mass flux relation and chemical phenomenon for Maxwell nanoliquid. Tangent hyperbolic nanofluid over stretched surface deliberated with the aspects of entropy generation and activation energy by Khan et al. [36]. Aspects of chemical mechanisms for 3D time-dependent flow of Maxwell fluid have been examined by Imtiaz et al. [37]. Khan et al. [38] considered the binary chemical reaction and activation energy for 3D cross-fluid.

Inspired by the overhead literature review, we have numerically computed the rheological behavior of cross-fluid subjected to revised heat flux relation. Furthermore, convective conditions are accounted in the modeling. More specifically, such features of cross-fluid have not yet been addressed in the literature. Numerical procedure is employed for simulations. Nature of significant parameters is elaborated graphically.

2. Modeling

Let us formulate 2D time-dependent radiative flow of incompressible cross-fluid subjected to convectively heated surface. Moreover, coordinate frame in this physical problem is chosen in such a manner that x-axis coordinates extend in direction of axial surface and r-axis is perpendicular to it which is shown in Fig. 1. More specifically, Lorentz's force is applied to control the motion of liquid. Besides, Brownian movement, radiation, thermophoresis, Brownian movement and convective conditions are accounted in the mathematical modeling. Furthermore, we have considered heated fluid at temperature T_f which is in contact with cylinder. An assumption is made that the sheet is in contact with a hot fluid at temperature T_f. The flow analysis of cross-liquid is carried out subject to chemical processes.

The analysis of quartic autocatalysis for isothermal process is given by

$$E + 2F \rightarrow 3F, \quad \text{rate} = k_1 G_a G_b^2, \tag{1}$$

while the catalytic surface for isothermal reaction in a single process and first order is

$$E \rightarrow F, \quad \text{rate} = k_s G_a, \tag{2}$$

Taking into consideration the aforesaid assumptions, the governing hydromagnetic flow of cross-fluid can be written into the forms given below:

$$\frac{\partial}{\partial x}(ru) + \frac{\partial}{\partial r}(rv) = 0, \tag{3}$$

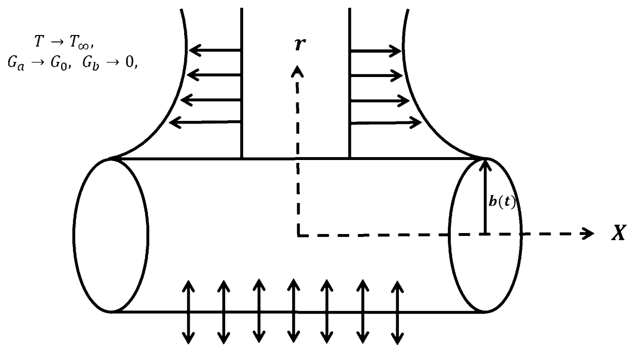

Fig. 1 Physical configuration

$$\frac{\partial u}{\partial t}+u\frac{\partial u}{\partial x}+v\frac{\partial u}{\partial r}=\frac{\partial U_{\mathrm{e}}}{\partial t}+U_{\mathrm{e}}\frac{\partial U_{\mathrm{e}}}{\partial x}+\frac{v}{r}\frac{\partial u}{\partial r}\left[\frac{1}{1+(\Gamma\frac{\partial u}{\partial r})^{n}}\right]+v\frac{\partial}{\partial r}\left[\frac{\frac{\partial u}{\partial r}}{1+(\Gamma\frac{\partial u}{\partial r})^{n}}\right]-\frac{\sigma^{*}B^{2}(t)}{\rho}(u-U_{\mathrm{e}}), \tag{4}$$

$$\frac{\partial T}{\partial t}+u\frac{\partial T}{\partial x}+v\frac{\partial T}{\partial r}=\alpha_{\mathrm{m}}\left[\frac{\partial^{2}T}{\partial r^{2}}+\frac{1}{r}\frac{\partial T}{\partial r}\right]-\frac{1}{(\rho c)_{\mathrm{f}}}\frac{\partial q_{\mathrm{r}}}{\partial r}+\frac{Q_{0}}{(\rho c)_{\mathrm{f}}}(T-T_{\infty}), \tag{5}$$

$$\frac{\partial G_{a}}{\partial t}+u\frac{\partial G_{a}}{\partial x}+v\frac{\partial G_{a}}{\partial r}=D_{A}\left(\frac{\partial^{2}G_{a}}{\partial r^{2}}+\frac{1}{r}\frac{\partial G_{a}}{\partial r}\right)-k_{1}G_{a}G_{b}^{2}, \tag{6}$$

$$\frac{\partial G_{\mathrm{b}}}{\partial t}+u\frac{\partial G_{\mathrm{b}}}{\partial x}+v\frac{\partial G_{\mathrm{b}}}{\partial r}=D_{\mathrm{B}}\left(\frac{\partial^{2}G_{\mathrm{b}}}{\partial r^{2}}+\frac{1}{r}\frac{\partial G_{\mathrm{b}}}{\partial r}\right)+k_{1}G_{\mathrm{a}}G_{\mathrm{b}}^{2}, \tag{7}$$

with

$$u=U_{\mathrm{w}}(x,t)=\frac{2cx}{1-\beta t},\ v=V_{\mathrm{w}}(t)=-\frac{ab_{0}s}{\sqrt{1-\beta t}},\quad k\frac{\partial T}{\partial r}=-h_{\mathrm{f}}[T_{\mathrm{w}}-T],\qquad D_{\mathrm{A}}\frac{\partial G_{\mathrm{a}}}{\partial r}=k_{\mathrm{s}}G_{\mathrm{a}},\quad D_{\mathrm{B}}\frac{\partial G_{\mathrm{b}}}{\partial r}=-K_{\mathrm{s}}G_{\mathrm{a}}\ \text{at}\ r=b(t) \tag{8}$$

$$u\to U_{\mathrm{e}}(x,t)=\frac{2ax}{1-\beta t},\quad T\to T_{\infty},\quad G_{\mathrm{a}}\to G_{0},\quad G_{\mathrm{b}}\to 0,\quad \text{as}\ r\to\infty, \tag{9}$$

where

$$q_{\mathrm{r}}=-\frac{16\sigma^{*}}{3k^{*}}T^{3}\frac{\partial T}{\partial r}. \tag{10}$$

Substituting Eq. (10) in Eq. (5), we get

$$\frac{\partial T}{\partial t}+u\frac{\partial T}{\partial x}+v\frac{\partial T}{\partial r}=\alpha_{m}\left[\frac{\partial^{2}T}{\partial r^{2}}+\frac{1}{r}\frac{\partial T}{\partial r}\right]+\frac{1}{(\rho c)_{f}}\frac{\partial}{\partial r}\left(\frac{16\sigma^{*}}{3k^{*}}T^{3}\frac{\partial T}{\partial r}\right)+\frac{Q_{0}}{(\rho c)_{f}}(T-T_{\infty}), \tag{11}$$

Employ

$$u=\frac{2ax}{1-\beta t}f^{'}(\eta),\ v=-\frac{ab_{0}}{\sqrt{1-\beta t}}\frac{f(\eta)}{\sqrt{\eta}},\ \eta=\left(\frac{r}{b_{0}}\right)^{2}\frac{1}{1-\beta t},\quad \theta(\eta)=\frac{T-T_{\infty}}{T_{\mathrm{w}}-T_{\infty}},\ \phi(\eta)=\frac{G_{\mathrm{a}}}{G_{0}},\ \vartheta(\eta)=\frac{G_{\mathrm{b}}}{G_{0}}. \tag{12}$$

Equation (3) is justified trivially, whereas Eqs. (4)–(11) yield

$$\left[1+(1-n)\left(\mathrm{We}\,f^{''}\right)^{n}\right]f^{'''}\eta+\left[1+\left(1-\frac{n}{2}\right)\left(\mathrm{We}\,f^{''}\right)^{n}\right]f^{''}+\left[Re\left(ff^{''}-f^{'2}+1\right)-A\left(f^{'}+\eta f^{''}-1\right)-M^{2}Re\left(f^{'}-1\right)\right]\left[1+\left(\mathrm{We}\,f^{''}\right)^{n}\right]^{2}=0, \tag{13}$$

$$\eta\theta^{''}+(1+\mathrm{Pr}\,\mathrm{Re}f-\mathrm{Pr}\,A\eta)\,\theta^{'}+\frac{2}{3N_{\mathrm{R}}}\left[(1+(\theta_{\mathrm{w}}-1)\theta)^{3}\left(2\eta\theta^{''}+\theta^{'}\right)+6(1+(\theta_{\mathrm{w}}-1)\theta)^{2}(\theta_{\mathrm{w}}-1)\eta\left(\theta^{'}\right)^{2}\right]+\mathrm{Pr}\,\lambda\theta=0, \tag{14}$$

$$\frac{1}{\mathrm{Sc}}\left[\phi^{'}+\eta\phi^{''}\right]-A\phi^{'}\eta+\mathrm{Re}f\phi^{'}-K\phi\vartheta^{2}=0, \tag{15}$$

$$\frac{\varepsilon}{\mathrm{Sc}}\left[\vartheta^{'}+\eta\vartheta^{''}\right]-A\vartheta^{'}\eta+\mathrm{Re}f\vartheta^{'}+K\phi\vartheta^{2}=0 \tag{16}$$

$$f(1)=s,\ f^{'}(1)=\lambda_{1},f^{'}(\infty)\to 1, \tag{17}$$

$$\theta^{'}(1)=-\gamma[1-\theta(1)],\ \theta(\infty)\to 0, \tag{18}$$

$$\phi^{'}(1)=K_{\mathrm{s}}\phi(1),\ \phi(\infty)\to 1, \tag{19}$$

$$\varepsilon\vartheta^{'}(1)=-K_{\mathrm{s}}\vartheta(1),\ \vartheta(\infty)\to 0, \tag{20}$$

The mathematical forms of variables appearing in Eqs. (13)–(20) are expressed as follows

$$\mathrm{We}=\frac{2\Gamma rU_{\mathrm{e}}}{b_{0}^{2}(1-\beta t)},\ \mathrm{Pr}=\frac{v}{\alpha_{\mathrm{m}}},\ \mathrm{Sc}=\frac{v}{D_{\mathrm{B}}},\ A=\frac{b_{0}^{2}\beta}{4v},\quad Re=\frac{ab_{0}^{2}}{2v},\ \varepsilon=\frac{D_{\mathrm{B}}}{D_{\mathrm{A}}},M^{2}=\frac{\sigma B_{0}^{2}}{2\rho a}(1-\beta t),\ \lambda=\frac{Q_{0}}{a(\rho c)_{\mathrm{f}}},\quad \theta_{\mathrm{w}}=\frac{T_{\mathrm{w}}}{T_{\infty}},\ \lambda_{1}=\frac{c}{a},\ K=\frac{k_{1}G_{0}^{2}(1-\beta t)\,b_{0}^{2}}{4v}. \tag{21}$$

Dimensional forms of (C_{f}) and (Nu) are

$$C_{\mathrm{f}}=\frac{\tau_{rx}\,|_{r=b(t)}}{\frac{1}{2}\rho U_{\mathrm{e}}^{2}}, \tag{22}$$

$$\mathrm{Nu}=\frac{b(t)\,q_{\mathrm{w}}\,|_{r=b(t)}}{2k(t)\,(T_{\mathrm{w}}-T_{\infty})}+q_{\mathrm{r}}, \tag{23}$$

where

$$\tau_{rx} = \mu_0 \frac{\partial u}{\partial r} \left[\frac{1}{1 + \left(\Gamma \frac{\partial u}{\partial r}\right)^n} \right] \Bigg|_{r=b(t)}, \tag{24}$$

$$q_{\mathrm{w}} = -k \left(\frac{\partial T}{\partial r} \right) \Bigg|_{r=b(t)} + q_{\mathrm{r}}|_{r=b(t)}. \tag{25}$$

After the utilization of Eqs. (24) and (25), the simplified form of Eqs. (22) and (23) is

$$C_{\mathrm{f}} Re_x \frac{x}{b(t)} = f''(1) \left[1 + \left(\mathrm{We} f''(1) \right)^n \right]^{-1}, \tag{26}$$

$$\mathrm{Nu} = -\theta'(1) \left[1 + \frac{4}{3N_{\mathrm{R}}} \left\{ [1 + (\theta_{\mathrm{w}} - 1)\,\theta(1)]^3 \right\} \right] \tag{27}$$

where $Re_x = ax^2/\nu$.

3. Results and discussion

Our main emphasis in this section is to analyze the physical importance of involved parameters that directly affect the cross-liquid velocity, temperature and mass concentration fields. Furthermore, we have discussed the significance of rheological parameters on (C_{f}) and (Nu). More specifically, Figs. 2, 3, 4, 5, 6, 7, 8 and 9 are drafted to get insight

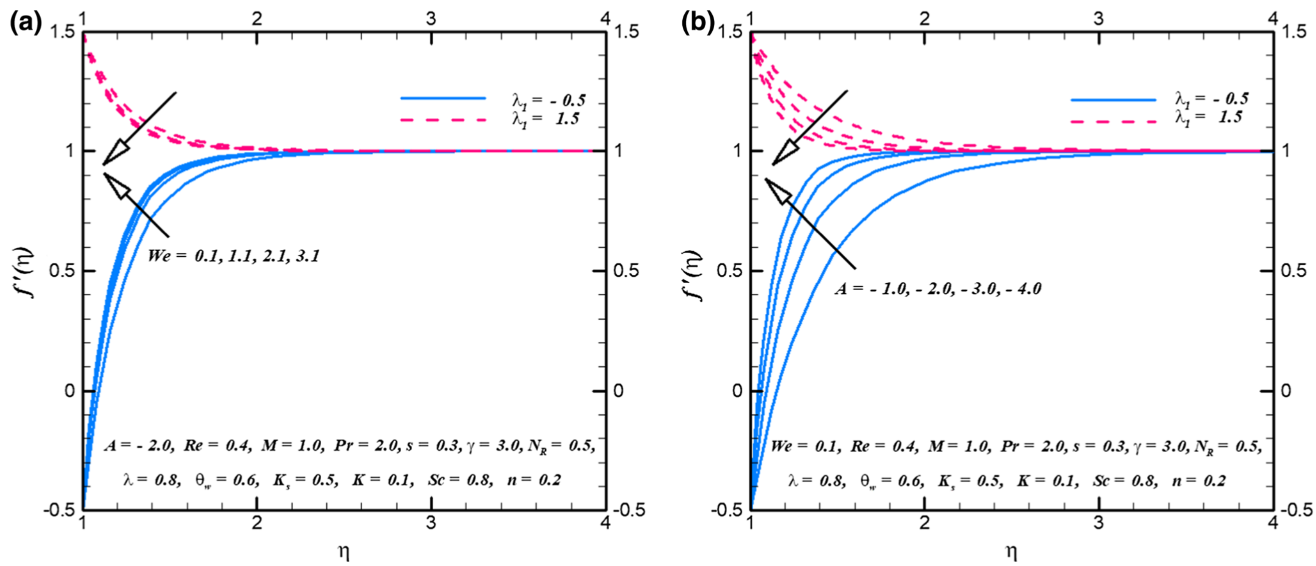

Fig. 2 (**a**), (**b**) $f'(\eta)$ profile via We and A.

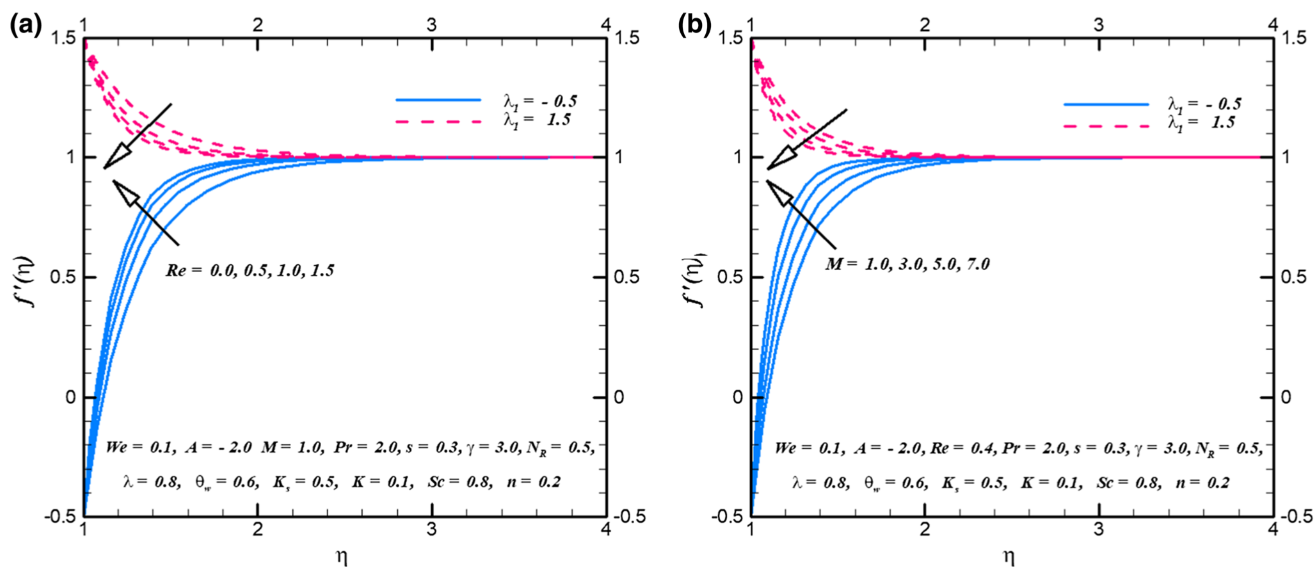

Fig. 3 (**a**), (**b**) $f'(\eta)$ profile via Re and M

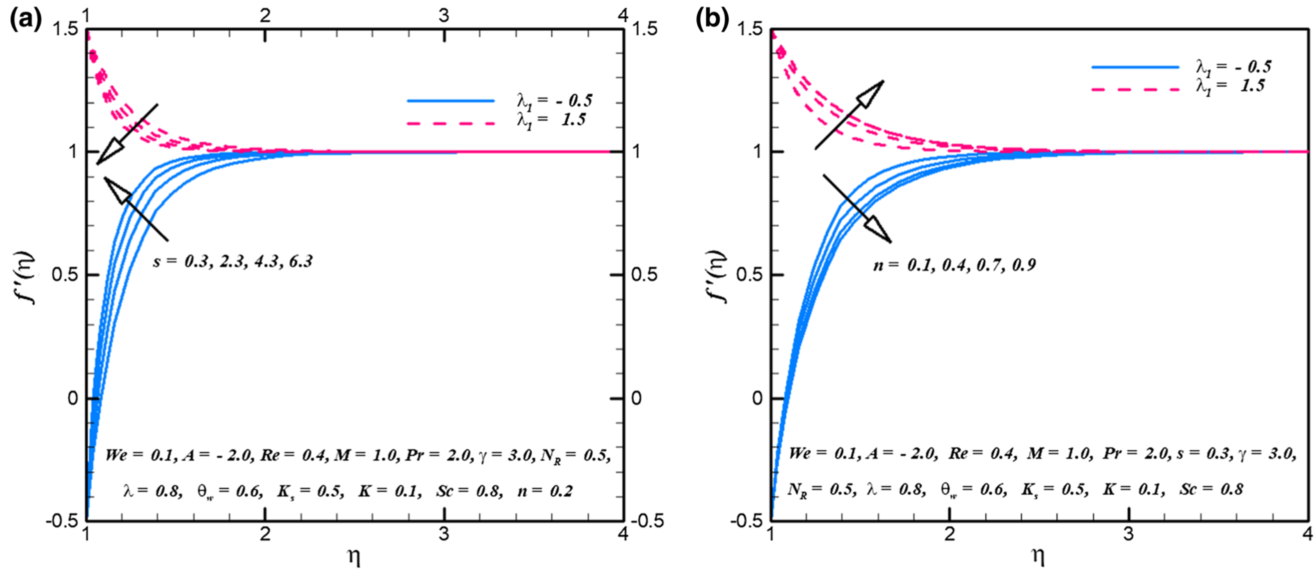

Fig. 4 (**a**), (**b**) $f'(\eta)$ profile via s and n

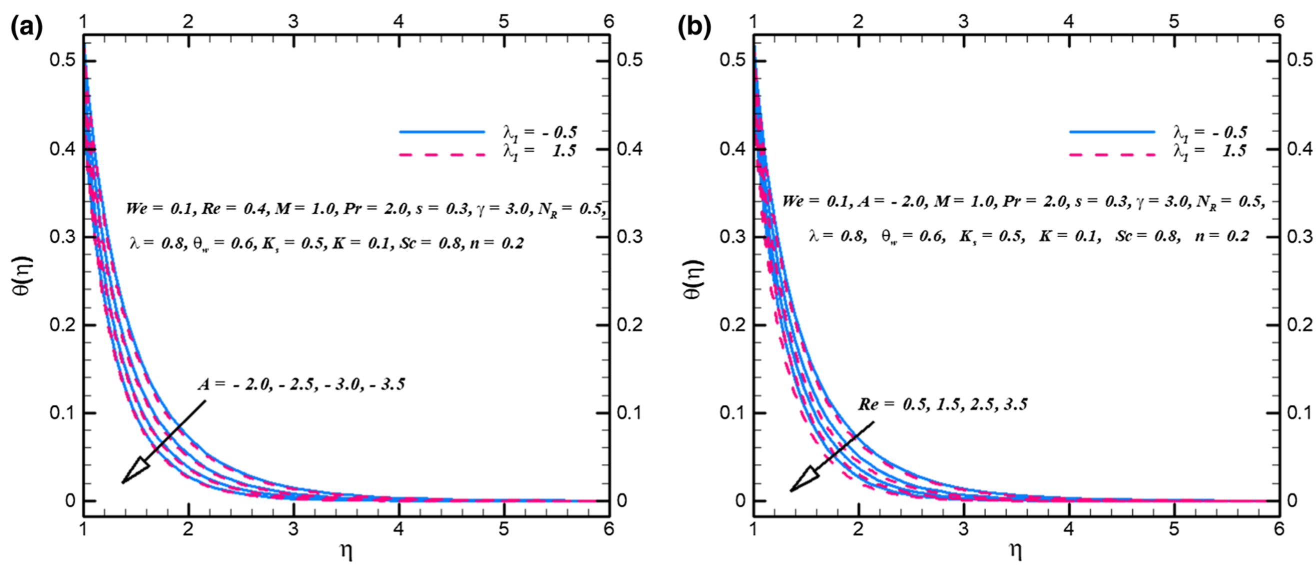

Fig. 5 (**a**), (**b**) $\theta(\eta)$ profile via A and Re

of the pertinent variables like local Weissenberg number (We), time-dependent parameter (A), suction parameter (s), power law index (n), thermal Biot number (γ), Reynolds number (Re), Prandtl number (Pr), radiation parameter (N_{R}), heterogeneous strength of reaction parameter (K_{s}) and Schmidt number (Sc).

Figure 2(a, b) is plotted for the physical importance of We and A on $f'(\eta)$ for stretching cylinder $(\lambda_1 = 1.5)$ and shrinking cylinder $(\lambda_1 = -0.5)$. Clearly, velocity of cross-liquid and associated layer thickness declines against We and A larger stretching cylinder $(\lambda_1 = 1.5)$, while liquid velocity rises against shrinking $(\lambda_1 = -0.5)$ case. From a physical point of view, We is ratio between relaxation time and specific process time. Consequently, rising estimations of We intensifies relaxation time as a result velocity of cross-liquid deteriorates for stretching cylinder $(\lambda_1 = 1.5)$. Impact of Re and M on $f'(\eta)$ is depicted in Fig. 3(a,b). From these figures, it is perceived that velocity of cross-liquid and momentum boundary layer rises against Re and M for shrinking cylinder $(\lambda_1 = -0.5)$ case, while opposite trend is detected for stretching cylinder $(\lambda_1 = 1.5)$. Physically, Lorentz's forces intensify with larger values of M. More specifically, Lorentz force acts as resistive force, which deteriorates the liquid velocity of cross-fluid. Figure 4(a, b) shows the behavior of suction parameter (s) and power law index (n) for $f'(\eta)$. Clearly, one can detect from graphical data that velocity of cross-liquid and associated layer thickness declines against larger suction parameter

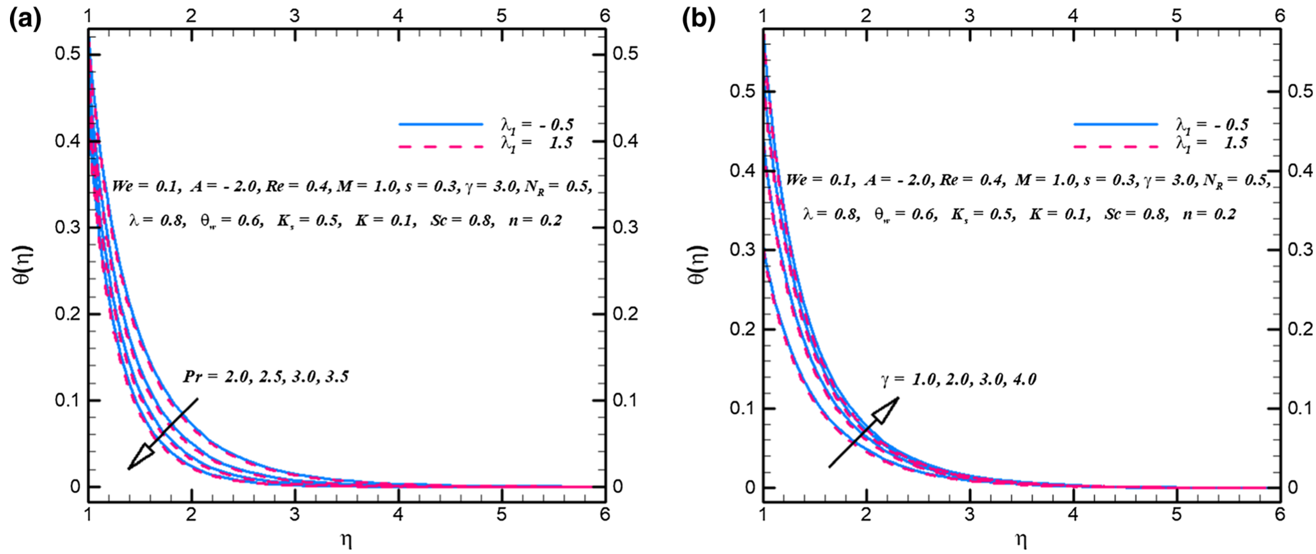

Fig. 6 (**a**), (**b**) $\theta(\eta)$ profile via Pr and γ.

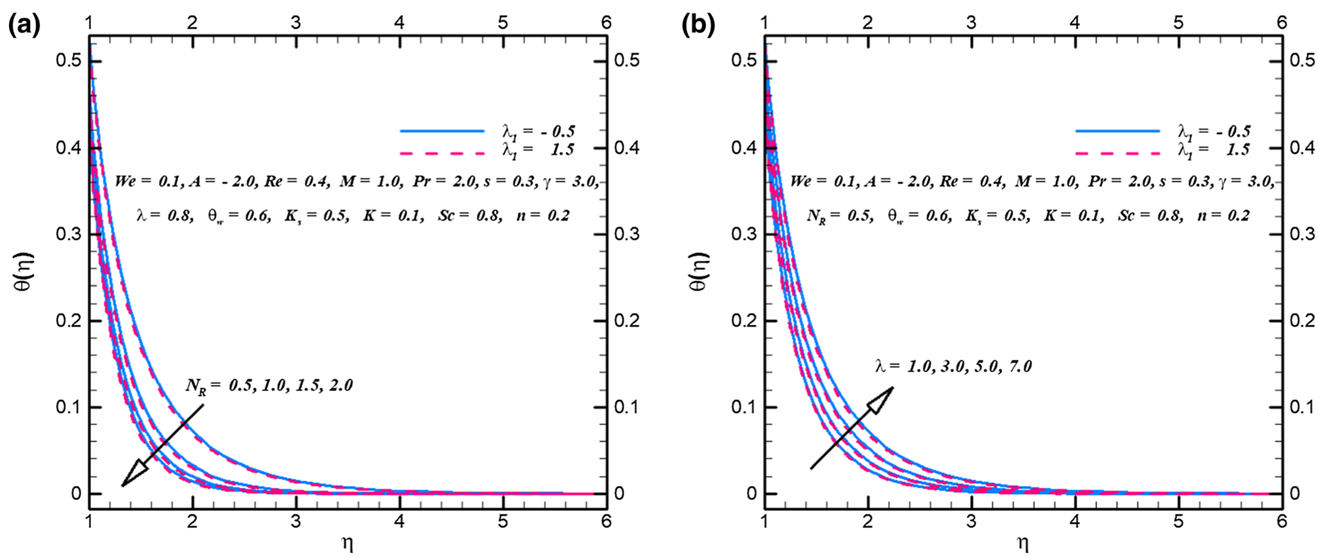

Fig. 7 (**a**), (**b**) $\theta(\eta)$ profile via N_R and λ

(s) for stretching cylinder ($\lambda_1 = 1.5$), while opposite phenomenon is detected for shrinking cylinder ($\lambda_1 = -0.5$). Moreover, it is observed that cross-liquid velocity $f'(\eta)$ boots via larger power law index (n) for stretching cylinder ($\lambda_1 = 1.5$), whereas reverse trend is detected for shrinking cylinder ($\lambda_1 = -0.5$).

Figure 5(a, b) elaborates the significance of A and Re on $\theta(\eta)$ for stretching ($\lambda_1 = 1.5$) and shrinking cylinder ($\lambda_1 = -0.5$). Decreasing trend of $\theta(\eta)$ is noticed for larger A and Re. Figure 6(a, b) discloses the characteristics of Pr and γ against $\theta(\eta)$. A rise in γ yields decreasing trend of $\theta(\eta)$, whereas reverse behavior of Pr via $\theta(\eta)$. From mathematical point of view, Pr is ratio between kinematic viscosity (momentum diffusivity) and thermal diffusivity. Consequently, thermal diffusivity of cross-liquids boosts for intensifying values of Pr as a result thermal field declines. Furthermore, for larger values of γ, less resistance is faced by the thermal wall which intensifies the convective mechanism of heat transportation. Features of N_R and λ against $\theta(\eta)$ are elaborated in Fig. 7(a,b). As expected, $\theta(\eta)$ and allied thermal layer increase with larger values of λ for stretching ($\lambda_1 = 1.5$) and shrinking cylinder ($\lambda_1 = -0.5$), while opposite behavior is detected against N_R. In fact, larger quantity of heat has produced due to an upsurge in heat generation parameter (λ). Therefore, thermal field ($\theta(\eta)$) rises.

Figure 8(a, b) delineates the impact of A and Re on $\phi(\eta)$. For higher estimation of these non-dimensional

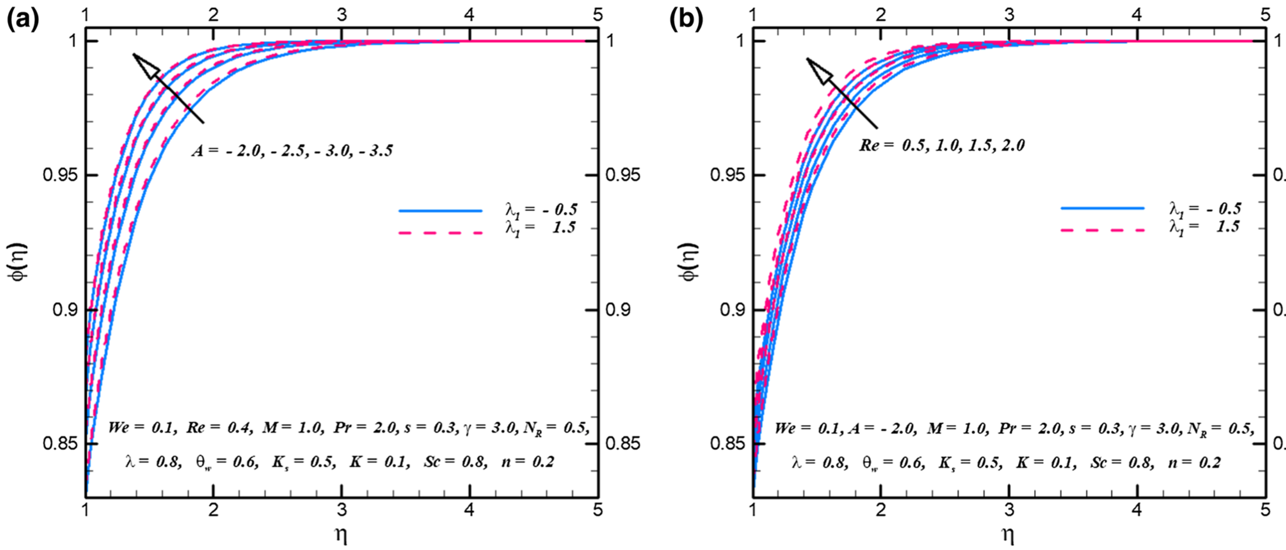

Fig. 8 (**a**), (**b**) $\phi(\eta)$ profile via A and Re

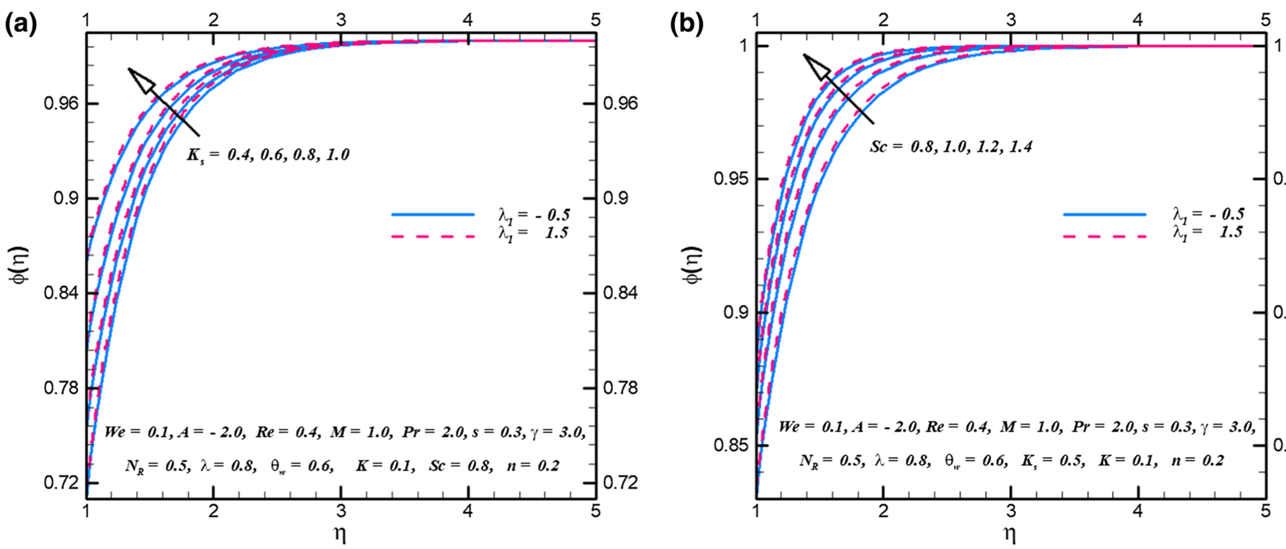

Fig. 9 (**a**), (**b**) $\phi(\eta)$ profile via K_s and Sc

parameters, the concentration of cross-liquid $\phi(\eta)$ rises. Figure 9(a,b) portrays the physical significance of K_s and Sc on concentration field of cross-liquid $\phi(\eta)$ for stretching $(\lambda_1 = 1.5)$ and shrinking cylinder $(\lambda_1 = -0.5)$. We have observed from these sketches that $\phi(\eta)$ intensifies for larger estimations K_s and Sc.

Numerical data for skin friction $\left(C_f Re \frac{x}{b(t)}\right)$ and Nusselt number (Nu) have been computed for stretching $(\lambda_1 = 1.5)$ and shrinking cylinder $(\lambda_1 = -0.5)$ in Tables 1 and 2. One can detect from Table 1 that $\left(C_f Re \frac{x}{b(t)}\right)$ boosted via M and Re, whereas $\left(C_f Re \frac{x}{b(t)}\right)$ deteriorates against A and M for shrinking cylinder $(\lambda_1 = -0.5)$. Furthermore, quite opposite trend of $\left(C_f Re \frac{x}{b(t)}\right)$ is observed for stretching $(\lambda_1 = 1.5)$ cylinder. Table 2 is prepared to visualize the characteristics of Nusselt number (Nu) against A, Pr, γ, θ_w, Re, M and N_R. Clearly, (Nu) intensified via larger Pr, γ, θ_w, Re and M; however, it reduces through A.

4. Conclusions

The research work presented in this physical model elaborates the aspects of hydromagnetic cross-fluid by considering cylindrical surface. Moreover, convectively heated surface and nonlinear radiation effects were considered in

Table 1 Computational outcomes of surface drag forces $\left(Re^{1/2}C_{fx}\right)$

$f''(1)[1+(\mathrm{We}f''(1))^n]^{-1}$

Parameter				$n = 0.2$	
We	Re	A	M	$\lambda_1 = -0.5$	$\lambda_1 = 1.5$
1.0	0.1	− 1.0	0.8	2.879849	− 1.352741
1.2	–	–	–	2.801122	− 1.148663
1.4	–	–	–	2.736085	− 0.9599094
1.6	0.6	–	–	3.53635	− 0.6029977
–	0.9	–	–	3.888841	− 0.5617491
–	1.2	–	–	3.99712	− 0.5418398
–	–	− 0.8	–	1.61366	− 0.440769
–	–	− 0.5	–	1.26718	− 0.449922
–	–	− 0.3	–	1.07132	− 0.454193
–	–	–	1.0	2.704694	− 0.7808874
–	–	–	1.5	2.78006	− 0.766445
–	–	–	2.0	2.869552	− 0.7568112

Table 2 Computational outcomes for rate of heat transfer $(Re^{-1/2}\mathrm{Nu})$

$-\theta'(1)\left[1+\frac{4}{3N_R}\left\{[1+(\theta_w-1)\theta(1)]^3\right\}\right]$

Parameter						$n = 0.2$	
A	Re	θ_w	M	Pr	N_R	$\lambda_1 = -0.5$	$\lambda_1 = 1.5$
2.0	0.4	0.6	0.1	0.2	0.5	1.43235	1.44138
1.5	–	–	–	–	–	1.3693	1.38056
1.0	–	–	–	–	–	1.30226	1.31666
0.5	0.6	–	–	–	–	1.24453	1.26944
–	0.9	–	–	–	–	1.26586	1.29801
–	1.2	–	–	–	–	1.28758	1.20895
–	–	0.8	–	–	–	1.3104	1.33015
–	–	1.0	–	–	–	1.34413	1.3633
–	–	1.3	–	–	–	1.3659	1.38184
–	–	–	0.5	–	–	1.23121	1.24963
–	–	–	0.8	–	–	1.23174	1.24953
–	–	–	1.0	–	–	1.23217	1.24944
–	–	–	–	0.4	–	1.41561	1.44615
–	–	–	–	0.6	–	1.55763	1.59593
–	–	–	–	0.8	–	1.67177	1.71542
–	–	–	–	–	0.7	1.67521	1.70235
–	–	–	–	–	0.8	1.96419	1.99572
–	–	–	–	–	1.0	3.26356	3.31712

the problem formulation. We have following noteworthy outcomes from aforementioned analysis: stretching cylinder ($\lambda_1 = 1.5$), while liquid velocity rises against shrinking ($\lambda_1 = -0.5$)

- Cross-liquid velocity $\left(f'(\eta)\right)$ deteriorates for larger We, Re, M and A in case of stretching cylinder ($\lambda_1 = 1.5$), while the reverse trend is detected for shrinking ($\lambda_1 = -0.5$).
- Thermal field intensifies for heat generation and Biot number (γ).
- Larger (Pr) yields higher temperature $(\theta(\eta))$.
- An increment in Pr corresponds to lower temperature and larger heat transfer rate.
- The concentration profile was decreased with the higher values of the homogeneous reaction parameter k_1.
- Skin friction $\left(Re^{1/2}C_{fx}\right)$ decays via larger We and A, whereas it enhances when We and A are increased.

Acknowledgements This project was funded by the postdoctoral international exchange program for incoming postdoctoral students, at Beijing Institute of Technology, Beijing, China.

Compliance with ethical standards

Conflict of interest The authors have no conflict of interest.

References

[1] W A Khan, M Khan and R Malik *PLoS ONE* **9(8)** e105107 (2014)

[2] M Khan, W A Khan and A S Alshomrani *Int. J. Heat Mass Transf.* **101** 570 (2016)

[3] T Hayat, M I Khan, M Tamoor, M Waqas and A Alsaedi *Results Phys.* **7** 1824 (2017)

[4] M Khan, M Manzur and M Rahman *Results Phys.* **7** 3767 (2017)

[5] W A Khan, I Haq, M Ali, M Shahzad, M Khan and M Irfan *J. Braz Soc. Mech. Sci. Eng.* **40** 470 (2018)

[6] M Manzur, M Khan and M ur Rahman *Int. J. Mech. Sci.* **138-139** 515 (2018)

[7] F Sultan, W A Khan, M Ali, M Shahzad, M Irfan and M Khan *Pramana—J. Phys.* **92** 21 (2019)

[8] M Sheikholeslami and M K Sadoughi *Int. J. Heat Mass Transf.* **116** 909 (2018)

[9] W A Khan, A S Alshomrani, A K Alzahrani, M Khan and M Irfan *Pramana—J. Phys.* **91** 63 (2018)

[10] M Sheikholeslami and M Seyednezhad *Int. J. Heat Mass Transf.* **120** 772 (2018)

[11] M Sheikholeslami and H B Rokni *Int. J. Heat Mass Transf.* **118** 823 2018

[12] A S Alshomrani, M Zaka Ullah, S S Capizzano, W A Khan and M Khan *Arab. J. Sci. Eng.* **44 (1)** 579 (2019)

[13] M Sheikholeslami, M Jafaryar, A Shafee, Z Li and R Haq *Int. J. Heat Mass Transf.* **136** 1233 (2019)

[14] M Shruthy and B Mahanthesh *J. Nanofluids* **8 (1)** 222 (2019)

[15] M Sheikholeslami, R Haq, A Shafee, Z Lie, Y G Elaraki and I Tlili *Int. J. Heat Mass Transf.* **135** 470 (2019)

[16] B J Gireesha, M Archana, B Mahanthesh and B C Prasannakumara *Mult. Mod. Mater. Struct.,* **15 (1)** 227 (2019)

[17] M Irfan, W A Khan, M Khan and M M Gulzar *J. Phys. Chem. Solids* **125** 141 2019

[18] M Sheikholeslami, R Haq, A Shafee and Z Li *Int. J. Heat Mass Transf.* **130** 1322 (2019)

[19] M Khan, M Irfan, W A Khan and M Sajid *J. Braz. Soc. Mech. Sci. Eng.* **41** 116 (2019)

[20] I L Animasaun, O K Koriko, K S Adegbie, H A Babatunde, R O Ibraheem, N Sandeep and B Mahanthesh *J. Therm. Anal. Calorim.* **135 (2)** 873 (2019)

[21] M Sheikholeslami *Comput. Methods Appl. Mech. Eng*. **344** 319 (2019)

[22] S Z Abbas, W A Khan, H Sun, M Ali, M Irfan, M Shahzed and F Sultan *Appl. Nanosci.* (2019) https://doi.org/10.1007/s13204-019-01039-9

[23] M Sheikholeslami *Comput. Methods Appl. Mech. Eng.* **344** 306 (2019)

[24] M Ali, W A Khan, M Irfan, F Sultan, M Shahzed and M Khan *Appl. Nanosci*. (2019) https://doi.org/10.1007/s13204-019-01038-w

[25] M Sheikholeslami, M B Gerdroodbary, R Moradi, A Shafee and Z Li *Comput. Methods Appl. Mech. Eng*. **344** 1 (2019)

[26] M Sheikholeslami and Omid Mahian *J. Clean. Prod*. **215** 963 (2019)

[27] M Khan, M Irfan, W A Khan *Pramana-J. Phys*. **92** 17 (2019) https://doi.org/10.1007/s12043-018-1690-2

[28] A Nematpour Keshteli and M Sheikholeslami *J. Mol. Liq*., **274** 516 (2019)

[29] W A Khan, M Irfan, M Khan, A S Alshomrani, A K Alzahrani and M S Alghamdi *J. Mol. Liq.* **234** 201 (2017)

[30] M I Khan, M Waqas, T Hayat, M I Khan and A Alsaedi *J. Mol. Liq.* **246** 259 (2017)

[31] M A Sadiq, M Waqas and T Hayat *J. Mol. Liq.* **248** 1071 (2017)

[32] B Mahanthesh, B J Gireesha and P R Athira *Results Phys.* **7** 2375 (2017)

[33] T Hayat, M W A Khan, M I Khan, M Waqas and A Alsaedi *Phys. B.* **538** 138 (2018)

[34] M S Kumar, N Sandeep, B R Kumar and S Saleem *Alexandria Eng. J.* **57** 2027 (2018)

[35] G K Ramesh, S A Shehzad, T Hayat and A Alsaedi *J. Braz. Soc. Mech. Sci. Eng.* **40** 422 (2018)

[36] M I Khan, S Qayyum, T Hayat, M I Khan, A Alsaedi and T A Khan *Phys. Lett. A.* **382** 2017 (2018)

[37] M Imtiaz, A Kiran, T Hayat and A Alsaedi *J. Braz. Soc. Mech. Sci. Eng.* **40** 449 (2018)

[38] W A Khan, F Sultan, M Ali, M Shahzad, M Khan and M Irfan *J. Braz. Soc. Mech. Sci. Eng.* **4** 41 (2019)

Publisher's Note Springer Nature remains neutral with regard to jurisdictional claims in published maps and institutional affiliations.